J|A|C|S ARTICLES

Published on Web 08/10/2009

High-Resolution Cryogenic-Electron Microscopy Reveals Details of a Hexagonal-to-Bicontinuous Cubic Phase Transition in Mesoporous Silica Synthesis

Liora Omer,[§,‡] Sharon Ruthstein,[‡] Daniella Goldfarb,[‡] and Yeshayahu Talmon*[,§]

Department of Chemical Engineering, Technion-Israel Institute of Technology, Haifa 32000, Israel, and Department of Chemical Physics, Weizmann Institute of Science, Rehovot 76100, Israel

Received April 21, 2009; E-mail: ishi@tx.technion.ac.il

Abstract: We studied the structural evolution during the formation of large-pore cubic $Ia\bar{3}d$ silica-based mesoporous materials, synthesized with Pluroinc P123 and butanol as structure directing agents. We used cryogenic high resolution scanning electron microscopy (cryo-HRSEM) and freeze-fracture-replication (FFR) transmission electron microscopy (TEM). Typically a silica precursor is added to an acid-catalyzed solution of Pluronic P123 and butanol. The latter serves as a cosolute, which can be added either at the beginning of the reaction, or after precipitation and the formation of a hexagonal phase. In this study we focused on the structural evolution from the hexagonal phase to the final cubic phase in the two different reactions. The same structural evolution with different kinetics was detected for both reactions. Cryo-HRSEM and FFR-TEM images revealed that from the hexagonal phase a perforated layer (PL) phase is formed, which later evolves into a bicontinuous structure. The final cubic phase forms within the layers, maintaining their orientation. We suggest a formation mechanism involving cylinder merging for the hexagonal to PL transition. Upon additional polymerization of the silica, the PL phase relaxes into the stable $Ia\bar{3}d$ cubic phase. Another minor mechanism detected involves the direct transition between the hexagonal to the final cubic phase through cylinder branching.

Introduction

Ordered mesoporous materials with large-pore diameters of 2−30 nm and various symmetries can be synthesized using triblock poly(ethylene oxide)−poly(propylene oxide)−poly(ethylene oxide) copolymers (Pluronics, $PEO_xPPO_yPEO_x$).[1,2] These commercially available block-copolymers are low-cost, nontoxic and biodegradable surfactants. The mesoporous products display high structure regularity, thick inorganic walls, and excellent thermal and hydrothermal stability.[1] The most studied mesoporous material synthesized using Pluronics is the two-dimensional (2-D) hexagonal SBA-15,[2] which has been tested for many applications, some of these have been summarized in a number of studies and reviews.[3−8]

Three-dimensional (3-D) large-pore mesostructures are highly attractive for applications requiring easily accessible and uniform large pores. The $Ia\bar{3}d$ double-gyroid structure with its highly branched and interwoven bicontinuous structure is particularly attractive for applications which are susceptible to pore blockage.[9,10] The gyroid morphology of the $Ia\bar{3}d$ cubic phase is composed of a matrix constructed over the Schoen G minimal surface and two interpenetrated networks embedded in this matrix.[11] Wei and Hilhouse showed that the diffusion through a mesoporous thin film of cubic symmetry is more efficient than through 2D hexagonal and rhombohedral films.[12] Furthermore, they found that the diffusion through the double-gyroid phase was the highest among the cubic thin films by over an order of magnitude.[12] Large-pore cubic $Ia\bar{3}d$ mesostructured silica can be obtained with Pluronics using additives such as inorganic salts,[13,14] hydrophobic silica precursor (organosiloxane),[15,16] or

[§] Technion-Israel Institute of Technology.
[‡] Weizmann Institute of Science.

(1) Zhao, D. Y.; Huo, Q. S.; Feng, J. L.; Chmelka, B. F.; Stucky, G. D. *J. Am. Chem. Soc.* **1998**, *120* (24), 6024–6036.
(2) Zhao, D. Y.; Feng, J. L.; Huo, Q. S.; Melosh, N.; Fredrickson, G. H.; Chmelka, B. F.; Stucky, G. D. *Science* **1998**, *279* (5350), 548–552.
(3) Ispas, C.; Sokolov, I.; Andreescu, S. *Anal. Bioanal. Chem.* **2009**, *393* (2), 543–554.
(4) Attard, G. S.; Glyde, J. C.; Goltner, C. G. *Nature* **1995**, *378* (6555), 366–368.
(5) Vallet-Regi, M. A.; Ruiz-Gonzalez, L.; Izquierdo-Barba, I.; Gonzalez-Calbet, J. M. *J. Mater. Chem.* **2006**, *16* (1), 26–31.
(6) Edler, K. J. *Aust. J. Chem.* **2005**, *58* (9), 627–643.
(7) Epping, J. D.; Chmelka, B. F. *Curr. Opin. Colloid Interface Sci.* **2006**, *11* (2−3), 81–117.
(8) Ruthstein, S.; Goldfarb, D. In *Electron Paramagnetic Resonance*; Gilbert, B. C., Davies, M. J., Murphy, D. M., Eds.; RSC Publishing: Cambridge, 2008; pp 184−213.
(9) Sakamoto, Y.; Kim, T. W.; Ryoo, R.; Terasaki, O. *Angew. Chem., Int. Ed.* **2004**, *43* (39), 5231–5234.
(10) Landry, C. C.; Tolbert, S. H.; Gallis, K. W.; Monnier, A.; Stucky, G. D.; Norby, F.; Hanson, J. C. *Chem. Mater.* **2001**, *13* (5), 1600–1608.
(11) Mareau, V. H.; Akasaka, S.; Osaka, T.; Hasegawa, H. *Macromolecules* **2007**, *40* (25), 9032–9039.
(12) Wei, T. C.; Hillhouse, H. W. *Langmuir* **2007**, *23* (10), 5689–5699.
(13) Flodstrom, K.; Alfredsson, V.; Kallrot, N. *J. Am. Chem. Soc.* **2003**, *125* (15), 4402–4403.
(14) Tang, J. W.; Yu, C. Z.; Zhou, X. F.; Yan, X. X.; Zhao, D. Y. *Chem. Commun.* **2004**, (19), 2240–2241.
(15) Huang, J. H.; Tian, G.; Wang, H. S.; Xu, L.; Kan, Q. B. *J. Mol. Cat. A: Chem.* **2007**, *271* (1−2), 200–208.
(16) Che, S. N.; Garcia-Bennett, A. E.; Liu, X. Y.; Hodgkins, R. P.; Wright, P. A.; Zhao, D. Y.; Terasaki, O.; Tatsumi, T. *Angew. Chem., Int. Ed.* **2003**, *42* (33), 3930–3934.

10.1021/ja903178f CCC: $40.75

cosolutes such as anionic cosurfactants[17,18] with or without swelling agents,[19] or butanol.[9,20,21] The latter synthesis uses Pluronic P123 and *n*-butanol as structure-directing agents. The high quality large mesoporous $Ia\bar{3}d$ product, designated KIT-6, is obtained reproducibly at a relative large range of compositions of silica source, surfactant and butanol.[20,21]

To rationally design mesosporous materials, the interplay of physical and chemical factors has to be considered, and the formation mechanism should be understood and established. For dilute surfactant systems, Monnier et al. were the first to suggest the cooperative formation mechanism of inorganic−organic interfaces that lead to the precipitation of the mesophases from the dilute solution, emphasizing the governing role of the surfactant packing and interface curvature in the selection of a particular mesophase.[22] Thereafter, many studies have focused on the formation mechanism of various types of mesoporous materials. Reviewing the progress in this specific direction of mesoporous materials research is beyond the scope of this article; the reader is referred to a number of recent papers and reviews that summarize the progress of the mechanism understanding over the years.[6−8,23−29]

Recently we have employed electron paramagnetic resonance (EPR) techniques combined with cryogenic transmission electron microscopy (cryo-TEM) methods to elucidate the formation mechanism of the bicontinuous cubic material KIT-6.[30] Following that in situ study we suggested a model based on the correlation between molecular events detected with the EPR techniques and the mesostructure evolution observed by cryo-TEM methods. At the beginning of the reaction, when the silica precursor is added, only spheroidal micelles are present, and condensation of silica oligomers takes place at the micellar/water interface and inside the corona of the micelles. This condensation causes depletion of water and butanol from the micelles core toward their corona, leading to a decrease of curvature, followed by the elongation of the micelles into threadlike micelles (TLMs). At the end of that first stage of the reaction the TLMs form bundles. Around 150 min from the beginning of the reaction precipitation occurs. During the next stage of the reaction an accelerated condensation of silica in the precipitate is detected, associated with the formation of a hexagonal phase. In addition, water and butanol molecules diffuse from the corona to the corona/water interface, thus reducing the polarity of the corona, and promoting a curvature decrease at the last stage of the reaction, when a transition from the hexagonal to the cubic phase takes place. That last stage is thought to occur 6−24 h from the beginning of the reaction, after which the reaction mixture undergoes hydrothermal treatment (24 h at 100 °C). During that stage no changes were detected on the molecular level by EPR.[30] Although it is known that the system goes from the hexagonal phase to the bicontinuous cubic phase at the last stage of the reaction, understanding of the mechanism at that stage is lacking. Earlier studies on the 2D hexagonal SBA-15 material by the same methods revealed the same structural evolution leading to the hexagonal phase, though the evolution was faster for the SBA-15 synthesis, because of the higher acidity of the reaction mixture.[30,31] This similarity suggested that the major role of the butanol is after the formation of the hexagonal phase, and that it is not essential for the early stage of the reaction. Therefore, the synthesis of KIT-6 was modified, and butanol was added to the reaction mixture of SBA-15 after the hexagonal phase was formed.[30]

In this study we focus on the last stage of the formation of the cubic material, namely the transformation from the hexagonal phase. We studied both syntheses: the original KIT-6 synthesis[20] and the modified one, the SBA-15 synthesis procedure with butanol added some time after precipitation (henceforth designated as SBA-15+BuOH). We employed freeze-fracture-replication (FFR) transmission electron microscopy (TEM) and cryogenic high-resolution scanning electron microscopy (cryo-HRSEM). The precipitate cannot be studied by cryo-TEM because the samples are too thick. Che et al. were the first to use HRSEM for the study of mesoporous materials.[16,32] Recently Tüysüz et al. studied the surface topology of KIT-6, SBA-15 and MCM-41 mesoporous materials using HRSEM and DF-STEM (dark-field scanning-transmission electron microscopy) to obtain extremely high resolution. The real-space images of the examined mesoporous materials provided better understanding of pore topologies.[33] In the present work we studied by HRSEM using cryogenic techniques not the final dry and stable silica, but the silica gel still in solution, to elucidate intermediate structures during the synthesis. In addition to the dedicated equipment and technique one has to take into consideration that cryo-HRSEM specimens are electron-beam radiation-sensitive. Cryo-HRSEM is a novel methodology, allowing us direct imaging of nanostructures of soft materials in the bulk. By FFR-TEM we examined replicas of the fractured surfaces, while in the cryo-HRSEM we observed the fractured surfaces themselves. Both methods provide topological information of the fractured surface, though different nanostructured elements are accentuated due to the different contrast mechanisms of the two methods. We obtained unprecedented HR-SEM pictures of the vitrified specimen that together with the FFR-TEM results revealed that in both syntheses the $Ia\bar{3}d$ cubic

(17) Chen, D. H.; Li, Z.; Yu, C. Z.; Shi, Y. F.; Zhang, Z. D.; Tu, B.; Zhao, D. Y. *Chem. Mater.* **2005**, *17* (12), 3228–3234.
(18) Li, Z.; Chen, D. H.; Tu, B.; Zhao, D. Y. *Microporous Mesoporous Mater.* **2007**, *105* (1−2), 34–40.
(19) Chen, D. H.; Li, Z.; Wan, Y.; Tu, X. J.; Shi, Y. F.; Chen, Z. X.; Shen, W.; Yu, C. Z.; Tu, B.; Zhao, D. Y. *J. Mater. Chem.* **2006**, *16* (16), 1511–1519.
(20) Kim, T. W.; Kleitz, F.; Paul, B.; Ryoo, R. *J. Am. Chem. Soc.* **2005**, *127* (20), 7601–7610.
(21) Kleitz, F.; Choi, S. H.; Ryoo, R. *Chem. Commun.* **2003**, (17), 2136–2137.
(22) Monnier, A.; Schuth, F.; Huo, Q.; Kumar, D.; Margolese, D.; Maxwell, R. S.; Stucky, G. D.; Krishnamurty, M.; Petroff, P.; Firouzi, A.; Janicke, M.; Chmelka, B. F. *Science* **1993**, *261* (5126), 1299–1303.
(23) Palmqvist, A. E. C. *Curr. Opin. Colloid Interface Sci.* **2003**, *8* (2), 145–155.
(24) Ying, J. Y.; Mehnert, C. P.; Wong, M. S. *Angew. Chem., Int. Ed.* **1999**, *38* (1−2), 56–77.
(25) Wan, Y.; Zhao, D. Y. *Chem. Rev.* **2007**, *107* (7), 2821–2860.
(26) Flodstrom, K.; Wennerstrom, H.; Alfredsson, V. *Langmuir* **2004**, *20* (3), 680–688.
(27) Linton, P.; Alfredsson, V. *Chem. Mater.* **2008**, *20* (9), 2878–2880.
(28) Sundblom, A.; Oliveira, C. L. P.; Palmqvist, A. E. C.; Pedersen, J. S. *J. Phys. Chem. C* **2009**, *113* (18), 7706–7713.
(29) Linton, P.; Rennie, A. R.; Zackrisson, M.; Alfredsson, V. *Langmuir* **2009**, *25* (8), 4685–4691.
(30) Ruthstein, S.; Schmidt, J.; Kesselman, E.; Popovitz-Biro, R.; Omer, L.; Frydman, V.; Talmon, Y.; Goldfarb, D. *Chem. Mater.* **2008**, *20* (8), 2779–2792.
(31) Ruthstein, S.; Schmidt, J.; Kesselman, E.; Talmon, Y.; Goldfarb, D. *J. Am. Chem. Soc.* **2006**, *128* (10), 3366–3374.
(32) Che, S.; Lund, K.; Tatsumi, T.; Iijima, S.; Joo, S. H.; Ryoo, R.; Terasaki, O. *Angew. Chem., Int. Ed.* **2003**, *42*, 2181–2185.
(33) Tüysüz, H.; Lehmann, C. W.; Bongard, H.; Tesche, B.; Schmidt, R.; Schuth, F. *J. Am. Chem. Soc.* **2008**, *130* (34), 11510–11517.

phase evolved from the hexagonal phase through a perforated layer (PL) phase, which later on evolved into a bicontinuous structure.

Experimental Section

Syntheses. Reagents used for the syntheses: Pluronic P123 ($EO_{20}PO_{70}EO_{20}$, M_{av} = 5800, Aldrich), tetraethoxy-orthosilane (TEOS, $(CH_3CH_2O)_4Si$, 98 wt %; Aldrich), tetramethoxy-orthosilane (TMOS, $(CH_3O)_4Si$, 99 wt % Fluka), hydrochloric acid (HCl 32 wt %; Frutarom), butanol (BuOH 99.7 wt %; Aldrich).

KIT-6 was synthesized according to the procedure reported by Kim et al.[20] A typical KIT-6 synthesis was as follows: to a 36 mL of aqueous solution containing 1.0 g of P123 (0.172 mmol) 2.1 mL of HCl 32% (21.4 mmol) and 1.25 mL of BuOH (13.7 mmol) were added. The mixture was stirred for 1 h, followed by the addition of 2.3 mL (10.1 mmol) of TEOS. The time of TEOS addition was denoted $t = 0$. The resulting mixture was left under stirring for 24 h at 35−40 °C. Then, a sample was taken for preparation of FFR-TEM or cryo-HRSEM specimen. The remaining gel solution was heated at 100 °C for 24 h without stirring (hydrothermal treatment, HT). The solid product was recovered by filtering and dried at ambient atmosphere. The molar composition of the synthesis gel was: 1 TEOS: 0.017 P123: 2.12 HCl: 198 H_2O: 1.36 BuOH.

The SBA-15+BuOH synthesis route, previously suggested by Ruthstein et al.,[30] was as follows: To 16 mL of aqueous solution containing 0.5 g of P123 (0.086 mmol), 2.5 mL of HCl 32% (25.4 mmol) was added. After 20 min of stirring at 35 °C, 0.8 mL of TMOS (5.3 mmol) was added. The TMOS addition time was denoted $t = 0$. After 24 min 0.7 mL of BuOH (7.6 mmol) was added, when a hexagonal phase existed in the precipitant but the silica was not fully polymerized.[30] The resulting mixture was left under stirring for 24 h at 35 °C. Then, a sample was taken for preparation of FFR-TEM or cryo-HRSEM specimens. The remaining gel solution was heated at 100 °C for 24 h without stirring. The solid product was recovered by filtering and dried at ambient atmosphere. The molar composition of the synthesis gel was: 1 TMOS: 0.016 P123: 4.8 HCl: 188.7 H_2O: 1.43 BuOH. The organic template was removed in both syntheses by calcination at 500 °C for 3 h, preceded by gradual heating for 5 h.

Methods. The specimen preparation procedures for FFR-TEM and for cryo-HRSEM are similar, as illustrated in Figure 1. Specimen preparation was performed with a BAF-060 system (BalTec AG, Liechtenstein). A small drop of the sample was placed on an electron microscopy copper grid and sandwiched between two gold planchettes. The "sandwich" was plunged into liquid ethane at its freezing point, transferred into liquid nitrogen, and inserted into a sample fracture block, precooled by liquid nitrogen. The block was inserted into the BAF-060 vacuum chamber, maintained at −160 to −170 °C, and was split open to fracture the frozen sample drop. The fracture surfaces were etched by heating to −100 °C and immediate cooling back to −150 °C. The following steps differ for FFR-TEM and for cryo-HRSEM samples.

For FFR samples the surfaces were shadowed at a 15° angle with a 2 nm layer of platinum−carbon (Pt−C) to enhance topographic details, followed by perpendicular deposition of a 20 nm thick carbon layer for mechanical stability. The replicas were retrieved from the thawed samples, cleaned first in hydrofluoric acid 6% (prepared from HF 38−40%, Merck) and then in double-distilled water, mounted on TEM grids, and examined in the FEI T12 TEM operated at 120 kV at room temperature. Images were recorded digitally by a Gatan high-resolution US1000 cooled-CCD camera with the DigitalMicrograph software package. Fast Fourier transforms (FFTs) of the images were calculated by the DigitalMicrograph software.

Cryo-HRSEM samples were prepared by producing fast-frozen fractured surfaces in the same way as for the FFR. After etching at −100 °C, a Pt−C conductive thin film of 4 nm was deposited on the surfaces (at a 90° angle) to prevent charging of the surface by the electron beam. The coated specimens were transferred under vacuum by a BalTec VCT100 shuttle, precooled with liquid nitrogen, into a Zeiss Ultra Plus HRSEM, equipped with a Schottky field-emission electron gun and with a BalTec VCT100 cold-stage maintained at −150 °C. Specimens were examined at very low electron acceleration voltage (1 to 3.5 kV) and short working distance (2.9−3.3 mm) for high-resolution imaging of surface nanostructures. We used both the InLens and the Everhart−Thornley secondary electron imaging detectors.

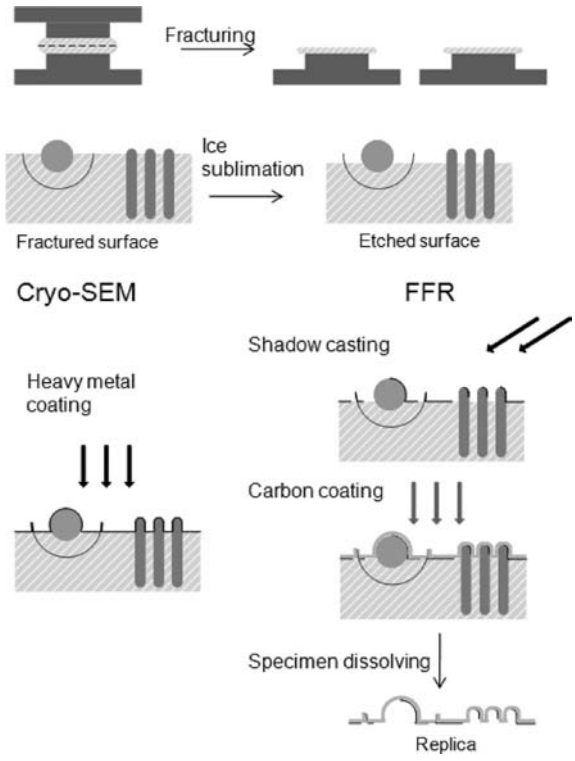

Figure 1. Illustration of specimen preparation procedures. All the steps, except replica retrieval, are performed at cryogenic temperature under vacuum.

Samples of the final materials were prepared for TEM by dispersing the powders in 1:1 EtOH/water solution, followed by 30 min of sonication. Then drops of the dispersion were deposited on a carbon/collodion-coated 300 mesh copper grid and were air dried. To prepare specimens for HRSEM we scattered the powder of the final material on a double-sided carbon conductive adhesive tape on an aluminum stub. We examined the TEM specimens by an FEI T12 TEM, and the HRSEM specimens by a Zeiss Ultra Plus HRSEM, as described above, at room temperature.

Results and Discussion

Both syntheses investigated produced ordered $Ia\bar{3}d$ cubic final material, as can be seen from the HRSEM picture and TEM micrographs shown in Figure 2. Micrographs A and B of Figure 2 are images of the cubic mesoporous material obtained with the KIT-6 synthesis, while Figure 2C is an image of the cubic material obtained with the SBA-15+BuOH synthesis. Insets are FFTs of the images, showing the cubic symmetry. The inset of Figure 2A corresponds to $Ia\bar{3}d$ cubic structure imaged along the [001] zone axis, and the insets in B and C fit the [111] zone axis. Typical small angle X-ray scattering (SAXS) patterns and nitrogen sorption isotherms are presented in Figures S1 and S2 in the Supporting Information. Those gave surface areas of 600 m^2/g, and cubic lattice parameter, a = 24 nm, in agreement with earlier studies.[20]

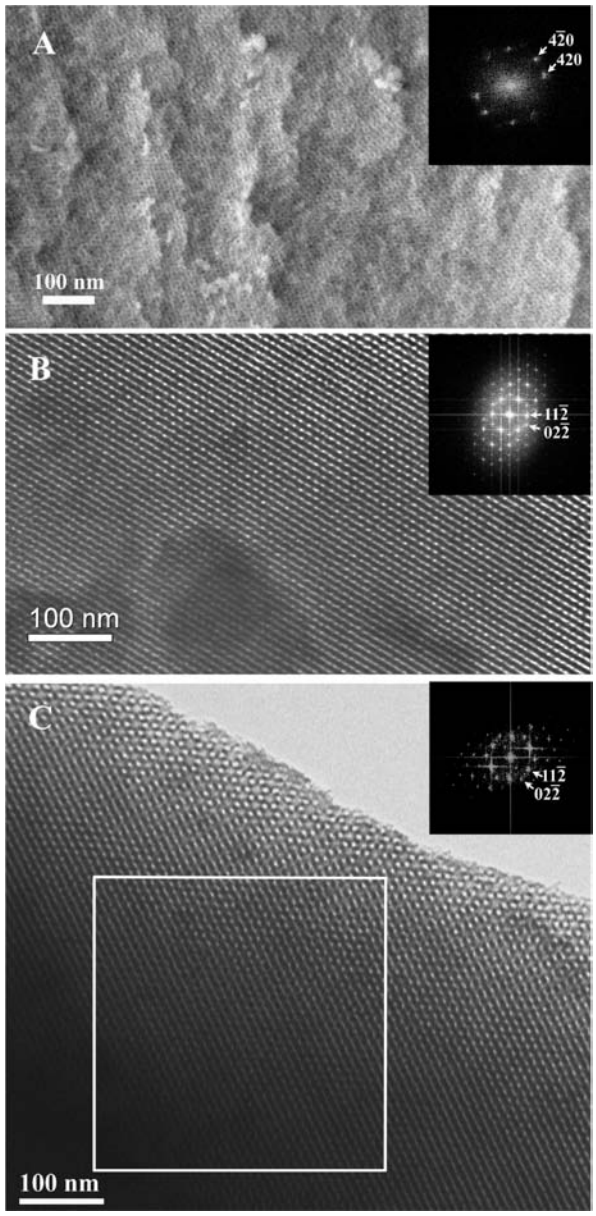

Figure 2. (A) HRSEM picture of dry cubic mesoporous silica before calcination, synthesized by the KIT-6 protocol. Inset is an FFT of this image showing that the cubic structure was imaged along the [001] zone axis. (B) and (C) TEM micrographs of calcined cubic mesoporous silica prepared by the KIT-6 synthesis, taken along [111] (B), and of the SBA-15+BuOH synthesis, taken along [111] (C). Insets are FFTs of the corresponding images.

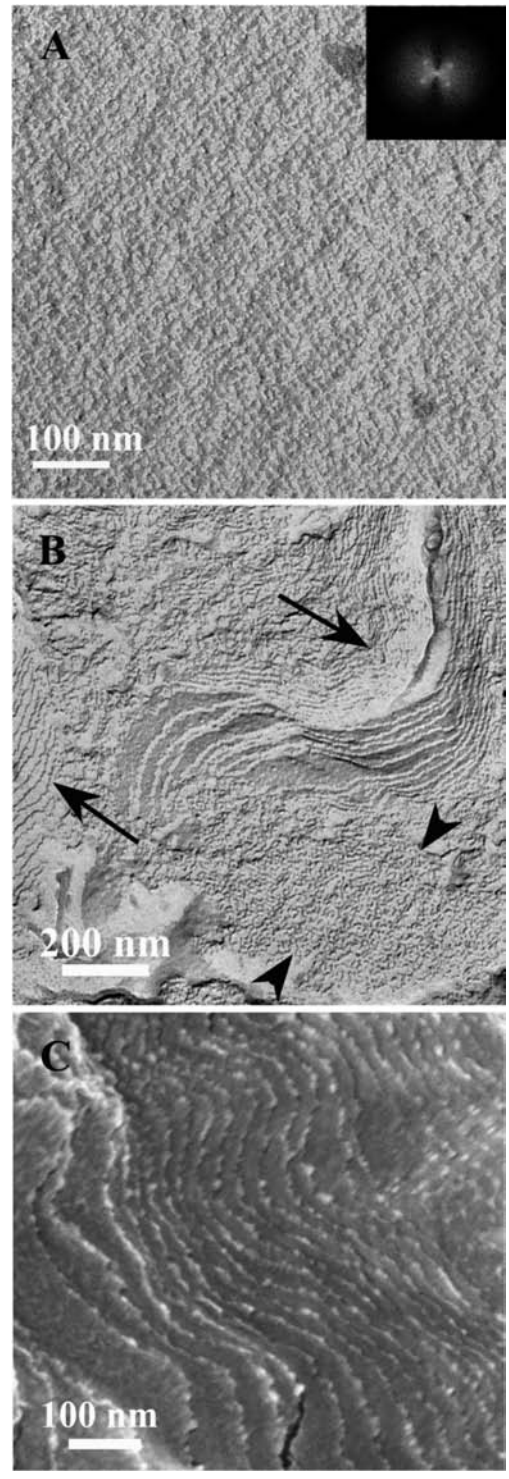

Figure 3. Images of KIT-6 synthesis solution before hydrothermal treatment. (A) FFR image showing a cubic structure. Inset is the FFT of the whole image. (B) FFR image showing semiordered bicontinuous phase marked by arrowheads, alongside layered phase (arrows). (C) Cryo-HRSEM image. The layered phase is clearly seen.

In general, both syntheses can be divided into two parts. In the first part the reaction mixture is stirred for 24 h at 35−40 °C. Then it undergoes hydrothermal treatment, during which the reaction mixture is kept at 100 °C for another 24 h. It is believed that the hydrothermal treatment acts to further polymerize the silica and to improve the order of the structures, namely, the structural evolution of the system is completed by the end of the first part.[30] Therefore, the reaction mixtures were sampled before the hydrothermal treatment, about 24 h from the beginning of the reaction, i.e. the addition of silica precursor to the mixture. Our main goal was to find out whether the structural evolution is indeed completed and a cubic structure is present, or whether the structural evolution continues into the hydrothermal treatment part, and possibly even into the drying process. After 24 h the synthesis mixtures were composed of precipitate in solution. To examine the wet precipitate without inducing artifacts or structural change by drying, we chose cryo-fixation, as discussed in the Experimental Section.

KIT-6 Synthesis. Two dominant phases were detected side-by-side in the reaction mixture before the hydrothermal treatment as shown in the FFR-TEM micrographs presented in A

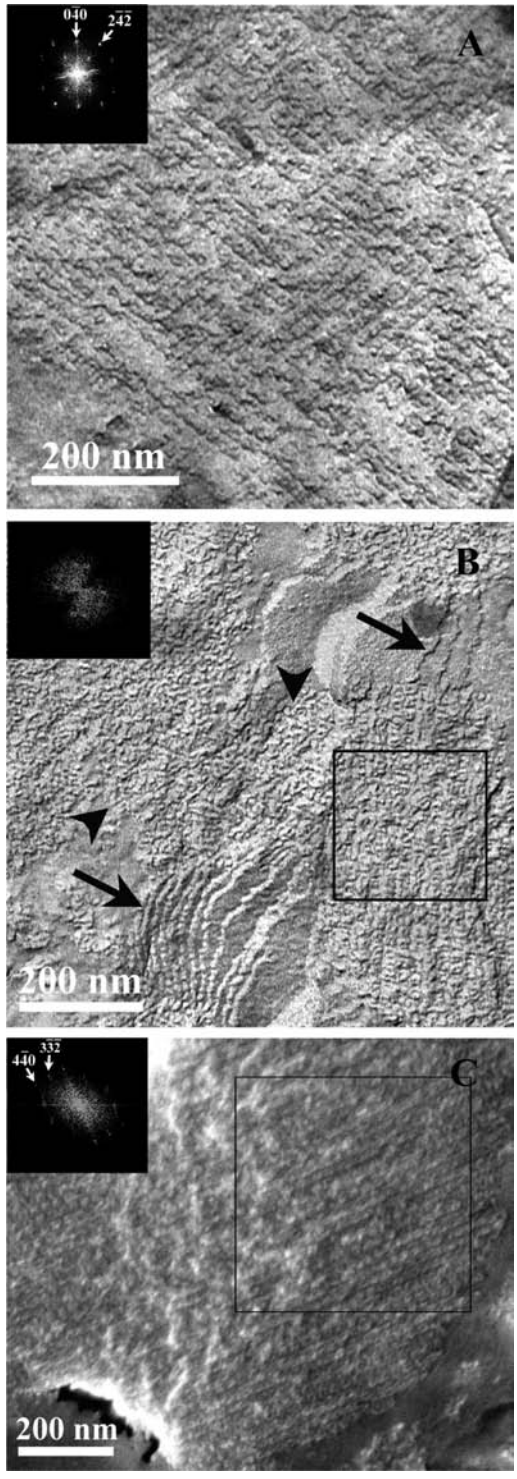

Figure 4. SBA-15+BuOH synthesis solution before hydrothermal treatment. FFR-TEM images of (A) cubic structure along [101] and (B) semiordered bicontinuous phase (arrowheads) alongside layered phase (arrows). (C) Cryo-HRSEM image. A cubic structure along [110] is seen. Insets are FFTs taken of the entire image or from the marked square area.

and B of Figure 3. Figure 3A shows an area where an ordered bicontinuous phase is seen. In Figure 3B we see flat layers of a lamellar phase, as indicated by arrows, alongside a bicontinuous phase with different degrees of order (arrowheads). A fracture through a disordered bicontinuous phase looks like a cut through a sponge, as seen in Figure 3B (arrowheads), and later in Figure 4B. We already know that the cubic phase in our systems is bicontinuous.[9,20] When the order is fully developed, we can verify it using FFTs of the images that show us the unique symmetry of the $Ia\bar{3}d$ bicontinuous cubic phase, as is the case in A and C of Figure 4. Cryo-HRSEM of the KIT-6 reaction mixture revealed the same structures, as presented in Figure 3C. However, in the cryo-HRSEM pictures it was easy to see that the layered structure is not simply a lamellar structure, but has an inner structure. This is clearly seen by the bright edges of the layers. After the detection of those "rough edged" layers with the cryo-HRSEM, these structures can be identified in the FFR-TEM images as well. In comparison, simple lipid bilayers have smooth edges, as we observed by cryo-HRSEM at comparable imaging conditions (unpublished work). Moreover, in FFR-TEM the contrast arises from the shadowing of the fractured surface, giving a 3-D topological effect. Similar information is obtained with cryo-HRSEM, where topological contrast is obtained by secondary electrons (SE) produced at the surface. More SE escape the surface at the edges of structures, thus marking edges with greater brightness.[34] This is an example for the complementarity of the two methods, emphasizing different structural elements and confirming the results by direct and indirect observation of the fractured surface. We observed a hexagonal phase only rarely (see below).

SBA-15+BuOH Synthesis. Similarly to the KIT-6 synthesis, bicontinuous structures with various degrees of order were seen here, alongside a layered structure (Figure 4). In this synthesis the most commonly encountered structure was the bicontinuous one, although the layered structure was also observed. The bicontinuous phase was in general more ordered than in the KIT-6 synthesis, as can be seen from the FFTs in the insets. In Figure 4A a cubic structure is imaged along the [101] zone axis, in Figure 4B the FFT shows that there is some order in the bicontinuous phase, but it is not fully developed into the cubic structure. In Figure 4C we see the cubic structure along [110]. No hexagonal phase was detected at this stage of the reaction. The cryo-HRSEM pictures of this specimen confirm those structures revealed by the FFR-TEM (Figure 4C).

This reaction mixture has higher acidity than the KIT-6 reaction mixture, leading to faster silica condensation and structural evolution.[1,31] This is demonstrated in the precipitation time and appearance of hexagonal phase in the two syntheses. While the precipitation time in the KIT-6 synthesis is around 150 min and the hexagonal phase first appears at around 4 h, the precipitation in the SBA-15 synthesis takes place after 18 min, and a hexagonal phase is detected in the precipitate already after 22 min.[30,31] Bearing this in mind, we suggest that those two syntheses go through the same structural evolution in the precipitate: (a) hexagonal phase → (b) layered structure → (c) disordered bicontinuous phase → (d) $Ia\bar{3}d$ cubic phase. When sampling the reaction mixtures at $t \approx 24$ h we capture different stages for each of the two reactions. The KIT-6 synthesis is captured at the stage of transition from (b) to (c), while the SBA-15+BuOH synthesis is at the transformation from (c) to (d). The better ordering of the bicontinuous phase in the SBA-15+BuOH synthesis, as well as the absence of hexagonal phase, supports this conclusion.

Kim et al.[20] preformed XRD measurements on materials dried at different stages of the synthesis, and proposed structural

(34) Goldstein, J. I.; Newbury, D. E.; Echlin, P.; Joy, D. C.; Lyman, C. E.; Lifshin, E.; Sawyer, L.; Michael, J. R. *Scanning Electron Microscopy and X-Ray Microanalysis*, 3rd ed.; Kluwer Academic/ Plenum Publishers: New York, 2003.

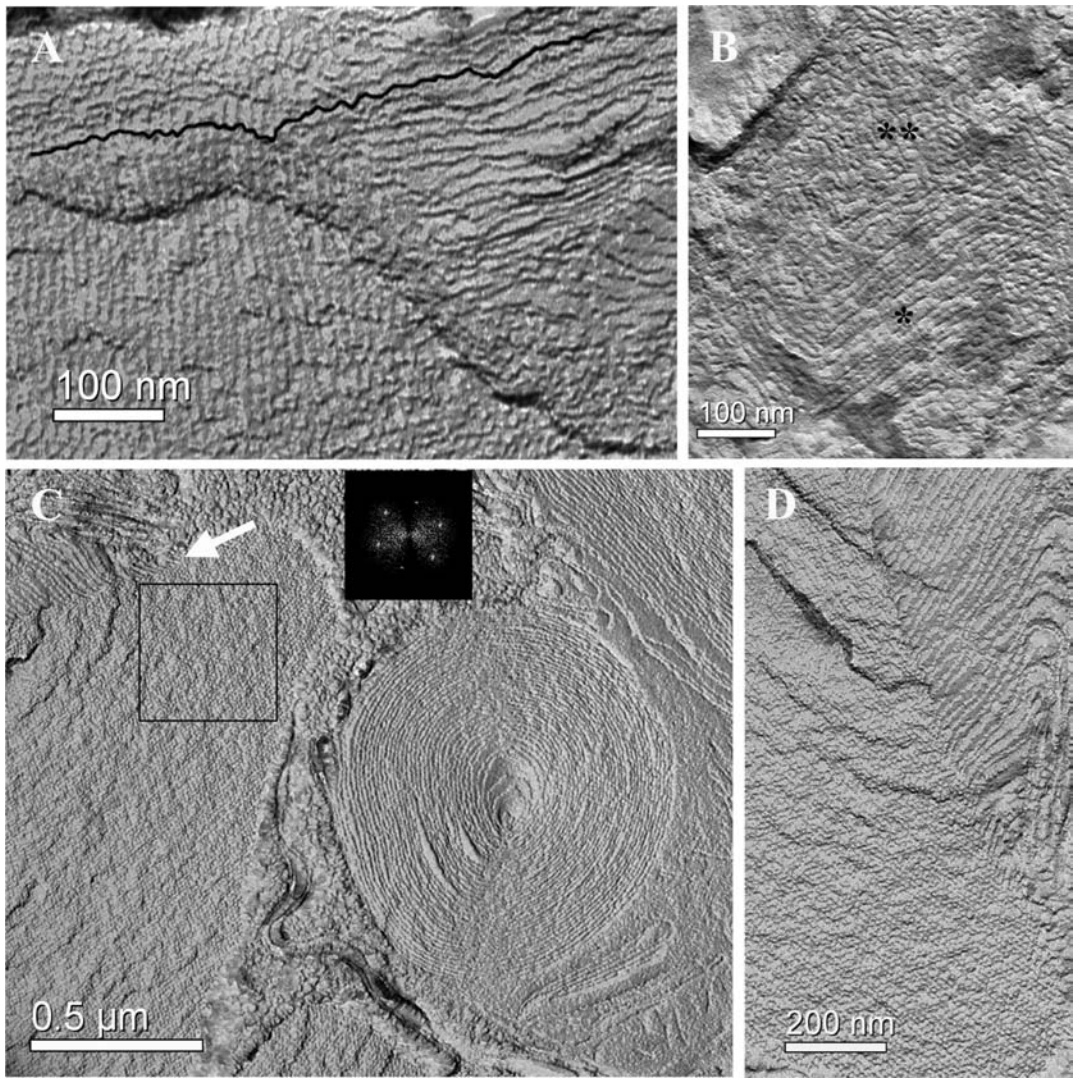

Figure 5. FFR-TEM images of the KIT-6 reaction solution before hydrothermal treatment. In (A), (C), and (D) a transition from the hexagonal to a layered phase is seen through cylinders merging along their short axis. In (A) a hexagonal phase is seen on the left, connected to a layered structure on the right. The black line marks one layer forming from one row of cylinders. In (C) a layered phase in the form of a vesicle is seen. The arrow marks an interface between hexagonal and layered structures. Inset in (C) is a FFT from the marked area showing a hexagonal symmetry. In (D) the layered structure in the right upper corner is connected to the hexagonal phase, seen through a fracture perpendicular to the long axis of the hexagonal phase. In (B) a transition between hexagonal phase (one asterisk), fractured along its long axis, to bicontinuous phase (two asterisks) is seen.

evolution from a lamellar phase to the bicontinuous cubic phase, although they did not detect the preceding hexagonal phase. This suggests that after the formation of the layered structure the system is not very sensitive to the drying process, meaning that at that stage of the reaction enough silica has polymerized to preserve the structure upon drying.

The Transformation Mechanism. Now that the structural evolution is established, the question of the transition mechanism between the different phases arises. To address that issue we focus on an area of two adjacent phases, seen in Figure 5. In A, C, and D of Figure 5 we see the hexagonal phase alongside the layered phase (note that the layered phase is made either of flat layers, or of layers closed upon themselves forming vesicles). Although FFR-TEM image analysis was previously done for different phases by us and by others,[30,31,35−38] we will elaborate on the image interpretation for the sake of clarity. The hexagonal phase in the FFR-TEM images can appear in three different forms, depending on the direction of the fracture in the hexagonal structure. When the structure is fractured along the long axis of the cylinders, the image shows uniform parallel lines. This is a more ordered and uniform structure than lamellae, which usually are fractured into terraces. Another possible fracture is perpendicular to the long axis of the cylinders; then the image appears as dots ordered in a hexagonal array. While a similar hexagonal symmetry may be seen for a cubic phase, fractured along the [111] direction, the cubic phase will not show the stack of lines (Figure 6 in reference 31)! When the fracture is in an arbitrary direction, the image shows stacks of cylinders broken into terraces, as seen in the left-hand side of

(35) Firouzi, A.; Kumar, D.; Bull, L. M.; Besier, T.; Sieger, P.; Huo, Q.; Walker, S. A.; Zasadzinski, J. A.; Glinka, C.; Nicol, J.; Margolese, D.; Stucky, G. D.; Chmelka, B. F. *Science* **1995**, *267* (5201), 1138–1143.
(36) Delacroix, H. *J. Microsc.* **1998**, *192* (Pt 3), 280–292.
(37) Maldonado, A.; Ober, R.; Gulik-Krzywicki, T.; Urbach, W.; Langevin, D. *J. Colloid Interface Sci.* **2007**, *308* (2), 485–490.
(38) Maldonado, A.; Lopez-Esparza, R.; Ober, R.; Gulik-Krzywicki, T.; Urbach, W.; Williams, C. E. *J. Colloid Interface Sci.* **2006**, *296* (1), 365–369.

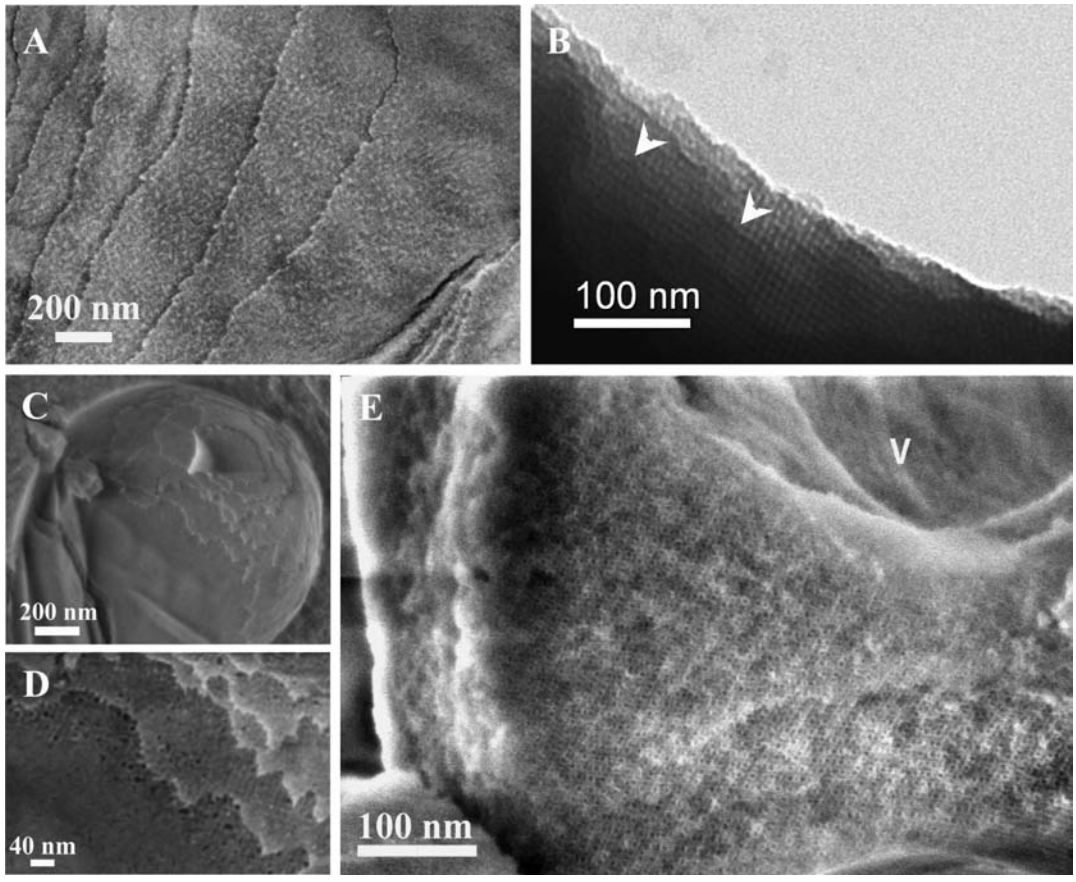

Figure 6. (A) Cryo-HRSEM of KIT-6 solution before hydrothermal treatment (HT). "Rough" layers with a texture indicative of inner structure are seen. (B) TEM micrograph of dry KIT-6 before HT shows layers, marked by arrowheads, with inner cubic structure. (C−E) HRSEM images of the KIT-6 material before calcination. In (C) a dry vesicle is seen. (D) is a high-magnification image of this vesicle after the electron beam had burned away the organic material, and revealed the cubic structure within the layers. (E) Cubic structure after irradiation of the shell of another vesicle. V marks the void within the vesicle.

Figure 5A. It seems that the transition from the stacked cylinders of the hexagonal phase to the layers occurs along the short cylinder axis. This is clear in Figure 5A, where the black line from left to right guides the eye along one row of cylinders transforming into one layer. The same transition is marked by the arrow in Figure 5C, and is also apparent in Figure 5D, where the layered structure in the right upper corner of the image is connected to the hexagonal phase. The inset in Figure 5C is an FFT of the marked square area of cylinders broken along their short axis, demonstrating that, indeed, this structure is of a hexagonal symmetry. A different, rarely observed, transition is seen in Figure 5B. Here we note a hexagonal phase (marked by one asterisk) connected to a disordered bicontinuous phase (marked by two asterisks). Here the hexagonal phase is fractured along its long axis. The connection seen here between the hexagonal and the bicontinuous phases suggests that a direct transition from the hexagonal phase to the bicontinuous phase, without going through the layered phase, is possible.

Landry et al.[10] described similar transitions from the hexagonal MCM-41 mesostructured material to the $Ia\bar{3}d$ cubic MCM-48 mesostructure by in situ XRD. Two mechanisms were proposed, "cylinder merging" and "cylinder branching". In the cylinder merging mechanism the curvature is lowered by connecting adjacent cylinders of the hexagonal phase along the cylinder axis to form sheets. This mechanism was used to explain the appearance of the transient lamellar phase in some of their experiments. The other mechanism of "cylinder branching" was initially proposed by Clerc et al.[39] for the hexagonal-to-$Ia\bar{3}d$ cubic phase transition in surfactant/water systems. This mechanism involves the formation of "monkey saddle" towers, i.e., minimal surfaces periodic in one dimension. To form such a tower from the hexagonal phase, the central cylinder in a group of seven is disrupted and serves to connect its six closest neighbors, three by three in alternate successive nodes, resulting in a bicontinuous structure composed of two separate and equivalent 3-D networks. The transition to the cubic $Ia\bar{3}d$ symmetry from this state is by a simple collective distortion of the monkey saddle structure. For the MCM-41 to MCM-48 transition it was concluded that the cylinder merging is reversible and kinetically favorable, while the cylinder branching is more favorable thermodynamically, but less reversible. Therefore, cylinder merging occurs in that system, but the transition to the cubic structure goes through cylinder branching.[10] This is not the case in our system. Though there is evidence for both mechanisms as discussed earlier, in all specimens we found a layered structure, thus indicating that this is the preferred intermediate structure of the system; hence, the cylinder merging mechanism is the dominant.

The unique cryo-HRSEM pictures show that the layered structure is not a simple lamellar phase. Figure 6A reveals that the rough-edged layers are not uniform and are textured, implying an inner structure. These findings can be explained

(39) Clerc, M.; Levelut, A. M.; Sadoc, J. F. *J. Phys. II Fr.* **1991**, *1* (10), 1263–1276.
(40) Hajduk, D. A.; Takenouchi, H.; Hillmyer, M. A.; Bates, F. S.; Vigild, M. E.; Almdal, K. *Macromolecules* **1997**, *30* (13), 3788–3795.

by a perforated lamellar structure (PL), a phase well-known in undiluted diblock-copolymers[40−42] and in diblock-copolymer/homopolymer blends,[11] and also recently found in an aluminosilicate templated by ABC triblock-copolymers.[43] The PL phase is composed of channels of the majority component (in our case the wet silica gel) extended through the minority component layers (the organic template). Moreover, this PL phase is known to be a metastable phase with frequently epitaxial relationship with the thermodynamically stable gyroid phase. In many systems the PL structure appears to be an intermediate structure which facilitates the formation of the gyroid phase.[11,40−42,44] This phase is also known in lyotropic liquid crystals as a 'mesh phase': an intermediate phase between the hexagonal and the lamellar phases, which competes with the gyroid phase, and shares its local structure and packing parameter (1/2−2/3).[45,46] The hexagonally perforated lamellar phase (HPL) and the gyroid phase possess nearly identical local structure, although the 3-D arrangement is very different: layered geometry for the HPL, in contrast to the 3-D networks of the gyroid. The similarity in local structure is responsible for the small difference in free energy, which drives the relaxation from the PL to the gyroid phase.[40,41] We could not distinguish the symmetry of the pores inside the layers using our methods, although it is probable that such symmetry exists, whether hexagonal symmetry as the origin phase, or cubic as the destination phase. Since the PL phase and the gyroid phase (of the final material) share similar curvature, the metastable PL phase preferentially relaxes to the gyroid phase, and not to the higher-curvature hexagonal phase. That explains the predominance of the cylinder-merging mechanism.

Further investigation of the layers by diverse microscopy methods reveals that the cubic structure grows within the layers of the PL phase. Figure 6B is a TEM micrograph of a material dried before the HT, showing the inner cubic structure of the layers. Images C−D of Figure 6 are HRSEM pictures of the final material before the removal of the organic material from the pores. Layered structure is seen in the form of vesicles (Figure 6C). Upon irradiation by the electron beam the organic material decomposes, exposing a cubic structure within the layers (D and E of Figure 6). Clerc et al.[39] proposed a cubic/lamellar transition mechanism which conserves the dense planes at the mesophase transitions. The formation of the bicontinuous cubic structure from the lamellar structure involves the introduction of channels into the lamellar structure. Every second organic surfactant layer is chosen to build one of the 3-D networks so that each layer is connected to its two next neighboring layers through holes in the closest layers. This transition seems natural in the PL phase which already contains the holes, enabling easy formation of the connectivity between the layers to form eventually the two organic networks in the minimal surface silica frame. After the removal of the organic compounds, the final material is obtained, a minimal surface silica frame with two pore networks, as beautifully visualized by Tüysüz et al.[33]

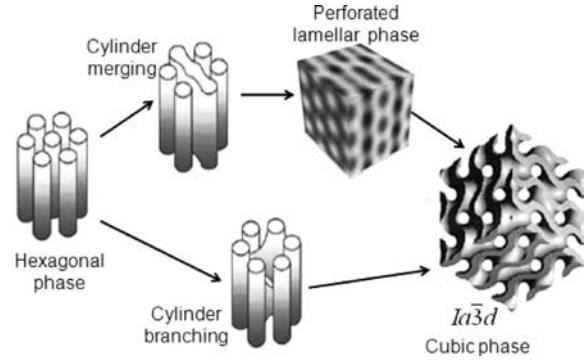

Figure 7. Proposed formation mechanism. The presented structure illustrations of hexagonal phase, cylinder merging, and cylinder branching are from Landry et al.,[10] PL from Qi and Wang,[42] and the $Ia\bar{3}d$ is from Wan and Zhao.[25]

To summarize, we propose for both syntheses a general structural evolution from the hexagonal phase to the final $Ia\bar{3}d$ cubic phase in two possible routes as illustrated in Figure 7. The cylinder branching route gives a direct transition to the bicontinuous phase, but it is a minor mechanism here. The dominant mechanism is cylinder-merging which forms the PL phase, later evolving to the bicontinuous phase within the layers.

Conclusions

We investigated, at the mesoscopic level, by cryo-electron microscopy techniques the final stages of the formation of an $Ia\bar{3}d$ cubic mesoporous material synthesized with Pluronic P123 and *n*-butanol, as structure-directing agents, in two different ways. Unique cryo-HRSEM pictures were obtained and, together with the FFR-TEM images, shed light on the structural evolution of the examined systems. It is shown that the main role of the butanol is in curvature lowering after the formation of the hexagonal phase. First, a hexagonal phase is formed, that further evolves into a perforated lamellar phase through cylinder merging. The final bicontinuous cubic structure evolves within the layers. Another minor mechanism in those systems involves the direct transition between the hexagonal to the final cubic phase through cylinder branching.

Acknowledgment. Financial support was received from the Petroleum Research Fund of the American Chemical Society. The microscopy was performed in the Technion Soft Matter Electron Microscopy Laboratory, supported by the Technion Russell Berrie Nanotechnology Institute (RBNI). D.G. holds the Erich Klieger Professorial Chair in Chemical Physics. This research is made possible in part by the historic generosity of the Harold Perlman Family. We thank Dr. Ellina Kesselman for her help in producing the FFR and cryo-HRSEM specimens, and our thanks goes to Dr. Rafail Khalfin for the SAXS measurements and analysis.

Supporting Information Available: XRD and nitrogen adsorption data of the final materials.This material is available free of charge via the Internet at http://pubs.acs.org.

JA903178F

(41) Forster, S.; Khandpur, A. K.; Zhao, J.; Bates, F. S.; Hamley, I. W.; Ryan, A. J.; Bras, W. *Macromolecules* **1994**, *27* (23), 6922–6935.
(42) Qi, S. Y.; Wang, Z. G. *Macromolecules* **1997**, *30* (15), 4491–4497.
(43) Toombes, G. E. S.; Mahajan, S.; Thomas, M.; Du, P.; Tate, M. W.; Gruner, S. M.; Wiesner, U. *Chem. Mater.* **2008**, *20* (10), 3278–3287.
(44) Mareau, V. H.; Matsushita, T.; Nakamura, E.; Hasegawa, H. *Macromolecules* **2007**, *40* (19), 6916–6921.
(45) Leaver, M.; Fogden, A.; Holmes, M.; Fairhurst, C. *Langmuir* **2001**, *17* (1), 35–46.
(46) Hyde, S. T.; Schroder, G. E. *Curr. Opin. Colloid Interface Sci.* **2003**, *8* (1), 5–14.